A New Model for Hard Braking Vehicles and Collision Avoiding Trajectories

Fynn Terhar

BMW Group
Department for Fleet Intelligence
Munich, Germany
Email: fynn.terhar@bmw.de

Christian Icking

FernUniversität in Hagen
Department for Cooperative Systems
Hagen, Germany
Email: christian.icking@fernuni-hagen.de

***Abstract*—In this paper, we propose a new model to describe vehicle dynamics in full braking situations with collision avoiding motions. By combining the equations of the classic Ackermann-Model with conditions that ensure a stable vehicle movement during simultaneous heavy braking and turning motions, we derive a model that describes the set of controllable trajectories. We describe these trajectories by compound motion equations in the x, y plane that are directly computable. We discuss our model regarding uncertainties and their effect on reachability analysis of vehicles in admissible scenarios, to show the feasibility of our solution. We compare our model to the well known Constant-Turn-Rate-And-Acceleration-Model which is computationally more expensive and less precise. By considering uncertainties of the parameters used in our model, we show a way to estimate the reachable area of a hard braking vehicle.**

Keywords–Reachability; Trajectory; Dynamic Vehicle Model; Safety; Collision Avoidance; Braking.

I. INTRODUCTION

A. Motivation

Many functions in Highly Automated Driving (HAD) and Advanced Driving Assistance Systems (ADAS) are discussed regarding their safety towards events caused by other traffic participants, whose behavior is not well predictable. In case of an unforeseen event, vehicles need to avoid a collision by a suitable trajectory. In literature, these trajectories are often referred to as Fail-Safe-Trajectories. These trajectories can either be evasive and try to find a solution around an obstacle or bring the vehicle to an emergency stop. The vehicle is then forced to find a trajectory till full stop within an area in front of the vehicle, which is defined by its physical properties and speed vector. In this paper, we call this area the *braking area*, which is important to know in many different applications. For example, when defining the set up of on-board sensors, it can be useful to have a good knowledge of the braking area. Also when searching for fail-safe trajectories, the knowledge of the reachable set of vehicle states can significantly accelerate the computation, as it reduces the search space and can therefore save valuable time in emergency situations.

B. Literature overview

Computing the braking area of a vehicle is related to finding fail-safe trajectories. Methods for avoiding obstacles are numerous, see for example Werling et al. [1], where the authors address dynamic street scenarios by an optimal control approach. The method generates trajectories that are optimal in terms of jerk minimization and following a previously computed trajectory. Another approach is explained by Ziegler et al. [2]. They use a cost function to plan obstacle avoiding paths in unstructured environments, but not on the description of fail-safe trajectories. Several approaches towards finding fail safe trajectories for road vehicles exist. Pek and Althoff [3] describe a method to generate fail-safe trajectories for dynamic traffic scenarios in a computationally efficient manner. Their solution approximates the set of reachable states of the ego vehicle and other traffic participants and can therefore guarantee collision free trajectories. A motion planner for fail-safe trajectories is shown by Magdici and Althoff [4]. A related application is presented in [5], where a safety framework is demonstrated that can test a planned trajectory for possible future collisions.

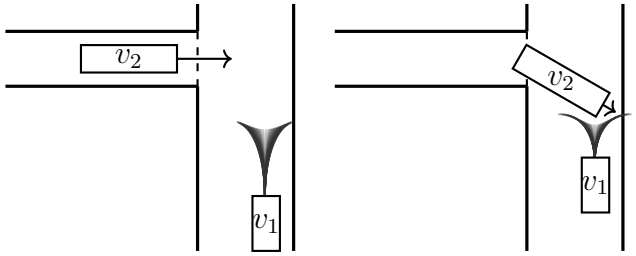

Figure 1. A critical traffic situation. Left, two vehicles approach a T-crossing without seeing each other. Right, vehicle v_1 is suddenly confronted with the long vehicle v_2 which blocks the road. To remain safe, v_1 should always know its reachable area in case of emergency braking.

Mitchell et al. [6] discuss different approaches of reachability analysis of dynamic systems for the safety assessment of trajectories. Asarin et al. [7] present an approach for reachability approximation of partially linearized systems in general. An often applied technique to approximate the state space efficiently is by zonotopes, see, e.g., the paper of Girad [8]. Koschi et al. [9] introduce an open source software solution which predicts road occupancy by traffic participants within a given time horizon. By overestimating the occupancy by the union of several object models, the authors ensure to find all possible traffic configurations. Potential braking and turning is overestimated by a circle of lateral and longitudinal maximum and minimum accelerations. The physical interaction between velocity and admissible lateral accelerations are therefore overestimated. Althoff [10] describes many underlying concepts of reachability analysis for road vehicles. In contrast to formal verification, ByeoungDo et al. [11] propose a Recurrent Neural Net for predicting traffic participants. Explicit braking and turning motions and their interrelation are not in the focus.

 ISBN: 978-1-61208-720-7

Our model provides a more detailed and accurate description of this interaction in order to reduce the overestimation towards a more realistic model.

The interrelation of braking and turning is, e.g., discussed by Giovannini et al. [12] where the authors describe the last point in time when a collision can be avoided by swerving. The authors explicitly focus their work on two-wheeled vehicles. Ackermann et al.[13] present control strategies for braking and swerving motions. Choi et al. [14] propose an additional strategy based on model predictive control.

C. Contribution

In this work, we present an accurate model for estimating not only a set of feasible trajectories of a vehicle while braking and turning till full stop. We also discuss the model regarding parameter uncertainties, to describe their effect on the overall *braking area*. Thereby, we aim to overestimate the occupancy where necessary, while reducing it where it is possible in order to provide both safety and accuracy.

In Section II, we define a model that directly calculates vehicle trajectories towards a full stop while simultaneously braking and steering. Braking and steering always needs to be done in a balanced way, as both influence the controllability of the vehicle on the road. We therefore introduce a parameter that describes the ratio of this compromise. Furthermore, the friction between different road surfaces and tires is considered, as well as the vehicles' dynamic limits and initial state. In Section III, we discuss how uncertainties of the model parameters influence the braking area. We thereby provide an estimation of the braking area in admissible situations.

II. Model definition

Physical model values are denoted as regular latin letters, while angles are denoted as greek letters. Symbols used in this paper are summarized in the following Table I:

TABLE I. Symbols used in this paper.

Symbol	*Description*	*Unit*
X_i	Model state at time i	–
p	Position $\in \mathbb{R}^2$	m
X_{stop}	Stop state, $v = 0$	–
ψ	Yaw Angle	rad
b	Braking Factor	–
$\hat{a}$	Maximum admissible acceleration	m/s^2
r_{turn}	Minimum turning radius	m
$\mathcal{I}_\bullet$	Interval of admissible values for $\bullet$	–
$\bullet_{\min}, \bullet_{\max}$	Extreme values of $\mathcal{I}_\bullet$	–
$\underline{f}(t), \overline{f}(t)$	Lower/Upper part of function $f(t)$	–

A. Assumptions

Our model builds upon assumptions that describe braking and turning in the following order of priority:

1) The vehicle needs to stop as quickly as possible.
2) By steering, the vehicle must try to avoid obstacles if ever possible, or minimize an unavoidable impact.

These assumptions hold in many situations where a collision can only be prevented by a full stop of the vehicle, as sketched out in Figure 1. Due to the high speed of v_2, the other vehicle v_1 can only react to the depicted incident by quickly stopping. The purpose of the following model is to predict the set of possible trajectories in space and time during braking maneuvers in such situations.

B. Model derivation

Our model builds on the so called *friction circle*, e.g. described by Pacejka [15]. As the modeled vehicle is braking in order to come to a full stop quickly, it will always be located near the boundary of this circle, either due to braking only, or by braking and turning in combination. Staying at the boundary of the friction circle means that the vehicle remains controllable in such an extreme maneuver. The basic concept of the friction circle is shown in Figure 2. The combined acceleration a_{res} is the vectorial sum of the centripetal acceleration $a_{\text{cen}} = v\underline{\dot{\psi}}$ and the longitudinal acceleration a_{lon}. An $a_{\text{res}} > \hat{a}$ can not be achieved, because the tires would loose their grip.

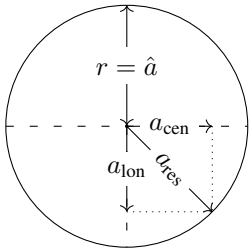

Figure 2. Friction circle in the a_x, a_y-plane. Radius r is equal to the maximally applicable acceleration $\hat{a}$ between vehicle and road surface.

Note, that the friction circle as shown in Figure 2 is an idealized and simplified model of tire forces. A more accurate model like the friction ellipse [15] will be implicitly considered in the reachability estimation in Section III, by introducing a high uncertainty in $\hat{a}$. The circle leads to the following equation:

$$a_{\text{res}} = \sqrt{a_{\text{cen}}^2 + a_{\text{lon}}^2} = \sqrt{(v\underline{\dot{\psi}})^2 + a_{\text{lon}}^2} \tag{1}$$

For a braking and turning maneuver in an emergency situation, we want to keep the vehicle controllable but also apply the strongest acceleration possible in order to react effectively. This constraints the vehicle to operate on the boundary of the friction circle, as described by (2).

$$\hat{a} = \sqrt{(v\underline{\dot{\psi}})^2 + a_{\text{lon}}^2} \tag{2}$$

1) Interrelation between braking, steering and yaw rate: The yaw rate $\dot{\psi}$ describes the change in yaw angle ψ of a vehicle over time. As the acceleration a_{res} results from a combination of braking and steering, the ratio $a_{\text{lon}}/\hat{a}$ causes different trajectories. We define this ratio by the factor b, as declared in (3), further on called *Braking Factor*. We call b Braking Factor, as it describes the percentage of $\hat{a}$ that is applied for braking rather than turning. A b value of -0.5 means that 50% of the applicable acceleration is applied for braking. Note, that $\hat{a}$ is positive, but when braking a_{lon} is negative, hence we choose $b \in [-1, 0]$.

$$b := \frac{a_{\text{lon}}}{\hat{a}} \tag{3}$$

Solving (2) for $\underline{\dot{\psi}}$ yields a description of $\underline{\dot{\psi}}(t)$, see (4).

$$\underline{\dot{\psi}}(t) = \frac{\hat{a}\sqrt{1 - b^2}}{v(t)} \tag{4}$$

Equation (4) describes the yaw rate $\dot{\underline{\psi}}(t)$ of a vehicle that stays at the boundary of the friction circle with radius $\hat{a}$. This describes the interrelation between braking, steering, and yaw rate.

2) Vehicle yaw angle as function of time: The vehicle's yaw angle ψ determines its travel direction, so a description of $\psi(t)$ is required for the model, as shown in (5).

$$\underline{\psi}(t) = \int \dot{\underline{\psi}}(t)dt = Z(\ln(v(t)) - \ln(v_0)) + \psi_0 \quad (5)$$

$$v(t) = a_{\text{lon}}t + v_0 \quad (6)$$

$$Z = b^{-1}\sqrt{1-b^2} \quad (7)$$

where $v(t)$ is the linear speed equation (6) and Z is a constant described by (7).

The angle $\underline{\psi}(t)$ rises in its absolute as the speed v falls. Figure 3 depicts this relation for an exemplary vehicle. The major flaw of this description is that the yaw rate tends towards ∞. This is not possible for any real vehicle, as the limit for a real vehicle is reached when the steering wheel reaches its maximum position and the minimum turning angle is performed. This effect is depicted in Figure 3 in the dashed line. As the speed approaches zero, $\underline{\psi}(t)$ approaches ∞. A realistic model must therefore respect the smallest *turning radius* r_{turn}. As $\dot{\psi}$ of a moving object is also defined as

$$\dot{\psi}(t) = \frac{v(t)}{r}$$

where r is the radius of the object's circular path, the maximal $\dot{\psi}(t)$ can be described by (8).

$$\dot{\overline{\psi}}(t) = \frac{v(t)}{r_{\text{turn}}} \quad (8)$$

By solving

$$\frac{\hat{a}\sqrt{1-b^2}}{a_{\text{lon}}t + v_0} = \frac{v(t)}{r_{\text{turn}}}$$

for t we know the time t_{crit} at which the yaw rate will reach its mechanical maximum, as shown in (9).

$$t_{\text{crit}} = \frac{\sqrt{r_{\text{turn}}\hat{a}\sqrt{1-b^2}} - v_0}{a_{\text{lon}}} \quad (9)$$

At times above t_{crit} we therefore describe the yaw angle by $\overline{\psi} = \int \dot{\overline{\psi}}(t)dt$, as shown in (10), in order to derive a realistic model.

$$\overline{\psi}(t) = \int \frac{v(t)}{r_{\text{turn}}}dt = \frac{\frac{1}{2}a_{\text{lon}}t^2 + v_0 t + const_{\overline{\psi}}}{r_{\text{turn}}} \quad (10)$$

where $const_{\overline{\psi}}$ must be defined in a way that the condition

$$\underline{\psi}(t_{\text{crit}}) = \overline{\psi}(t_{\text{crit}}) \quad (11)$$

holds. The condition means that the angle at t_{crit} must be equal for both (5) and (10). It yields $const_{\overline{\psi}}$ as:

$$const_{\overline{\psi}} = r_{\text{turn}}\underline{\psi}(t_{\text{crit}}) - \frac{1}{2}a_{\text{lon}}t^2 - v_0 t \quad (12)$$

The sectionally defined yaw angle ψ, consisting of $\underline{\psi}$ and $\overline{\psi}$, is plotted in Figure 3 (solid line). Note, how ψ now drops with falling speed, which directly follows from (8). The dashed line plots $\underline{\psi}(t)$, which approaches ∞ as the speed approaches zero. This follows from its property to be at the boundary of the friction circle. At low speeds, this can only be achieved by high yaw rates.

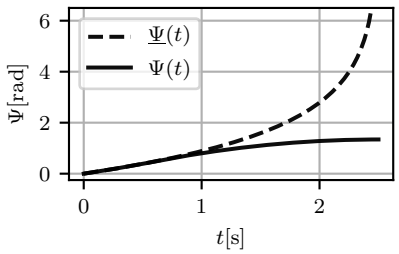

Figure 3. The yaw angle ψ over time t during braking and steering. Dashed line plots $\underline{\psi}(t)$. Solid line plots the combined stepwise definition $\psi(t)$ which considers the turning radius r_{turn} for $t > t_{\text{crit}}$.

The final description of $\psi(t)$ is defined stepwise in (13).

$$\psi(t) = \begin{cases} \underline{\psi}(t), & 0 \le t \le t_{\text{crit}} \\ \overline{\psi}(t), & t_{\text{crit}} < t \le t_{\text{stop}} \end{cases} \quad (13)$$

Note, that due to the equality condition of yaw angles in (11) and the definition of t_{crit} in (9) the final yaw angle $\psi(t)$ is differentiable. Also note, that then $t > t_{\text{crit}}$, the vehicle in our model is no longer at the boundary of the friction circle.

3) Vehicle position as function of time: A description of vehicle position $p(t) = [x, y]$ is described as the compound equations for x and y, which follow from the integrals:

$$x(t) = \int v(t)\cos(\psi(t))dt$$

$$y(t) = \int v(t)\sin(\psi(t))dt$$

Solving the integrals yields:

$$\underline{x}(t) = \frac{v(t)^2\,(Z\sin(\psi(t)) + 2\cos(\psi(t)))}{a_{\text{lon}}\,(Z^2+4)} + C_{\underline{x}} \quad (14)$$

$$\overline{x}(t) = r_{\text{turn}}\sin(\psi(t)) + C_{\overline{x}} \quad (15)$$

These equations describe position over time $x(t)$ and $y(t)$. See stepwise (16) for $x(t)$.

$$x(t) = \begin{cases} \underline{x}(t), & 0 \le t \le t_{\text{crit}} \\ \overline{x}(t), & t_{\text{crit}} < t \le t_{\text{stop}} \end{cases} \quad (16)$$

The constant $C_{\underline{x}}$ is bound by the conditions $x(0) = x_0$, which means the vehicle must be at the starting position at time t_0. The constant for $\overline{x}$, $C_{\underline{x}}$ is bound to hold the condition $\overline{x}(t_{\text{crit}}) = \underline{x}(t_{\text{crit}})$, which means that $\underline{x}$ must seamlessly – e.g. in value and gradient – be continued by $\overline{x}$ at t_{crit}. The result for both constants is described by (17) and (18).

$$C_{\underline{x}} = x_0 - \frac{v_0^2\,(Z\sin(\psi_0) + 2\cos(\psi_0))}{a_{\text{lon}}(Z^2+4)} \quad (17)$$

$$C_{\overline{x}} = x(t_{\text{crit}}) - r_{\text{turn}}\sin(\psi(t_{\text{crit}})) \quad (18)$$

 ISBN: 978-1-61208-720-7

The general description for $y(t)$ is shown below in (21), and can be derived analogously to $x(t)$.

$$\underline{y}(t) = -\frac{v(t)^2\left(Z\cos(\psi(t)) - 2\sin(\psi(t))\right)}{a_{\text{lon}}\left(Z^2+4\right)} + C_{\underline{y}} \tag{19}$$

$$\overline{y}(t) = -r_{\text{turn}}\cos(\psi(t)) + C_{\overline{y}} \tag{20}$$

$$y(t) = \begin{cases} \underline{y}(t), & 0 \le t \le t_{\text{crit}} \\ \overline{y}(t), & t_{\text{crit}} < t \le t_{\text{stop}} \end{cases} \tag{21}$$

$$C_{\underline{y}} = y_0 - \frac{v_0^2\left(Z\cos(\psi_0) - 2\sin(\psi_0)\right)}{a_{\text{lon}}(Z^2+4)}$$
$$C_{\overline{y}} = y(t_{\text{crit}}) + r_{\text{turn}}\cos(\psi(t_{\text{crit}}))$$

The trajectory of a braking and turning vehicle is described as $p(t)$, by the compound x- and y-position in Cartesian coordinates over time. How the more realistic yaw angle description influences the resulting position can be seen in a direct comparison in Figure 4. The vehicle performs a spiral shape until the maximum turning angle is reached, which is clearly visible in Figure 4b. In a real situation, this trajectory with such a low b value will most likely not be considered feasible for braking, it rather demonstrated the spiral nature of our model. Note, that all other $b \in]-1, 0[$ also describe spirals, only less clearly visible as in Figure 4a.

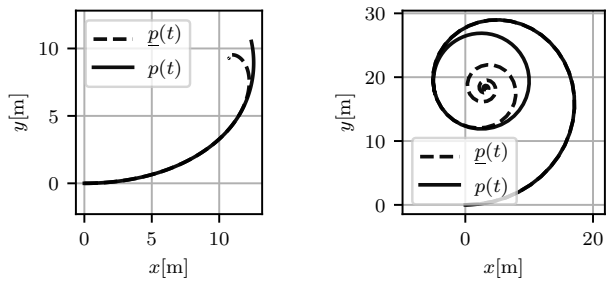

(a) Calculated position $p(t)$ with $b = -0.5$.

(b) Calculated position with $b = -0.085$.

Figure 4. Vehicle position $p(t)$ in x, y plane with different values for b. Dashed line, the model result without considering r_{turn}. Solid line, the model considering r_{turn}, using the final model equations.

In the next step, we compare our trajectories to simulative results of another model.

4) Comparison of our model against CTRA model: To evaluate our model's performance with respect to calculation time and to show its correctness, we compare it to a CTRA-model [16] *Constant Turn Rate and Acceleration* in a simulation. The CTRA simulation iteratively moves a vehicle, such that our condition in (2) is fulfilled, and the assumptions introduced in Section II hold. The simulation therefore calculates effectively the same maneuvers as our model, but in a very different way. We choose the CTRA-model, as it is well known, allows the vehicle to follow a spiral shape and has the same state space representation as our model. The turn rate and acceleration is assumed to be constant within one of many consecutive time steps Δt.

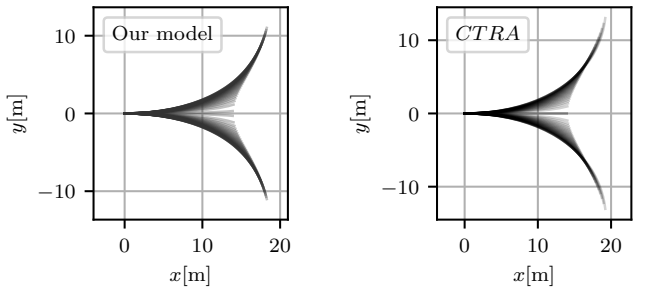

(a) Our braking model.

(b) CTRA model, $\Delta t = 0.0075s$.

Figure 5. Comparison of our model to the CTRA model for 40 vehicle trajectories with linearly sampled b values. The starting conditions for both tests are $v_0 = 16.67^m/_s, \hat{a} = 10^m/_{s^2}, r_{\text{turn}} = 12.5m, \psi_0 = 0\ rad$.

The result in Figure 5 shows that our model matches the shape of the CTRA-model well, without introducing linearization errors as the CTRA model does.

Both results from Figure 5 show a very similar structure. Note that the CTRA model (Figure 5b) has slightly longer trajectories, especially in the outer arms of the structure. This is caused by the CTRA-model's assumption of a constant turn rate $\dot{\psi}$, which is not correct in this kind of non-linear maneuver. In our model (Figure 5a), the only assumption is that of a constant acceleration, as introduced in Section II.

The main advantage of our model is the fact that we can directly compute certain vehicle positions straight from the formulas derived in Section II such that time intensive calculations are not necessary. A comparison of computation times t_{calc} in seconds, and their deviation $\sigma_{t_{\text{calc}}}$ over 10 runs is shown in Table II. In the first test, only the stop states where computed of 1000 different b values. In the second test, a whole pearl chain of positions from start to stop was computed, with 250 points per b value.

TABLE II. COMPARISON TO THE CTRA MODEL.

Calculate 1000 possible **stop states**, $\Delta t = 0.01112s$						
v_0	$5\ ^m/_s$		$10\ ^m/_s$		$20\ ^m/_s$	
	Mean t_{calc}[s]	$\sigma_{t_{\text{calc}}}$	Mean t_{calc}	$\sigma_{t_{\text{calc}}}$	Mean t_{calc}	$\sigma_{t_{\text{calc}}}$
CTRA	1.0715	0.0137	2.1975	0.0052	4.9310	0.1073
Our model	0.2059	0.0053	0.2078	0.0017	0.2144	0.0075
Calculate 1000 **trajectories**, 250 samples per trajectory, $\Delta t = 0.01112s$						
v_0	$5\ ^m/_s$		$10\ ^m/_s$		$20\ ^m/_s$	
	Mean t_{calc}	$\sigma_{t_{\text{calc}}}$	Mean t_{calc}	$\sigma_{t_{\text{calc}}}$	Mean t_{calc}	$\sigma_{t_{\text{calc}}}$
CTRA	1.0870	0.0207	2.2335	0.0096	4.9761	0.0814
Our model	0.2310	0.0017	0.2326	0.0021	0.2320	0.0011

The table shows that our model is up to 20 times faster in terms of computing time than the CTRA model, especially for high initial velocities v_0. This is caused by the fact that CTRA must iteratively compute time steps until the stop position is found, whereas our model can directly compute the stop state.

III. DISCUSSION OF MODEL UNCERTAINTIES

In this section, we discuss the effect of individual uncertainties in the model parameters $r_{\text{turn}}, \hat{a}$ and the initial vehicle state $X_0 = [x_0, y_0, v_0, \psi_0]^T$. We model the uncertainties as intervals $\mathcal{I}_\Theta$,$\mathcal{I}_{X_0}$ that contain all possible values.

A. Highest possible deceleration $\hat{a}$

The highest possible deceleration heavily depends on the road and tire conditions, which are often uncertain. The interval $\mathcal{I}_{\hat{a}}$ therefore covers the most slippery and most rough road condition possible. Calculating different stop states X_{stop} with different values for $\hat{a}$ reveals an almost linear behavior within expectable values of $\hat{a} \in \mathcal{I}_{\hat{a}}$.

The resulting shape of 50 different $\hat{a} \in \mathcal{I}_{\hat{a}}$ can be seen in Figure 6a, where lower values of $\hat{a}$ lead to a farther vehicle trajectory with an almost linear behavior.

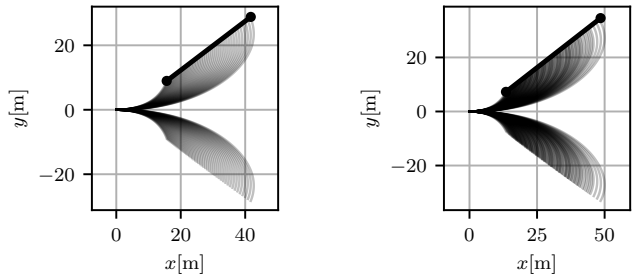

(a) Resulting trajectories at interval $\mathcal{I}_{\hat{a}} = [4, 12]\, m/s^2$.

(b) Resulting trajectories at intervals $\mathcal{I}_{\hat{a}} = [4, 12]\, m/s^2$, $\mathcal{I}_{v_0} = [15.3, 18.1]\, m/s$

Figure 6. Two sets of trajectories with a b value of -0.6. Left, only considering $\mathcal{I}_{\hat{a}}$. Right, considering $\mathcal{I}_{\hat{a}}$ and $\mathcal{I}_{v_0}$. A line segment shows the extending effect of the parameter uncertainties on the top half.

B. Smallest possible turning radius r_{turn}

The smallest possible turning radius r_{turn} is a vehicle inherent parameter which influences the trajectory after t_{crit} and also defines the value of t_{crit} itself. Although there are certain legal requirements for r_{turn} depending on vehicle class, the exact value is uncertain, especially when considering other traffic participants.

Any $r_{\text{turn}} \in \mathcal{I}_{r_{\text{turn}}}$ causes a different stopping position. Unfortunately, the lowest or highest $r_{\min}$ not always leads to the outmost stopping position. By observing the stopping positions depending on r_{turn}, one can see that the shape of all stopping positions with different $r_{\text{turn}} \in \mathcal{I}_{r_{\text{turn}}}$ forms a spiral with a rising radius. Let A be the stopping position of the lowest r_{turn}, $A = X_{\text{stop}}|_{r_{turn,min}}$, and $B = X_{\text{stop}}|_{r_{turn,max}}$. The circle with radius $r = dist(A, B)$ at center A then includes all points of the spiral, which means all stopping positions can be overestimated by such a circle. By describing this distance as function $d = f(\hat{a}, v_0)$, it can be shown that the maximum distance is at $d_{max} = f(\hat{a}_{min}, v_{0,max})$. Figure 7 shows an example of such a circle.

In order to show the spiral effect in Figure 7, we assumed $\mathcal{I}_{r_{\text{turn}}} = [1\text{e}{-7}, 13]m$ and $v_0 = 10^m/_s$, which results in a circle radius of $\approx 2.4m$. For a more realistic scenario of $\mathcal{I}_{r_{\text{turn}}} = [7, 13]m$ and $v_0 = 10^m/_s$, the radius of the circle is $\approx 1.3m$.

C. Initial velocity v_0

The uncertainty in the initial velocity $\mathcal{I}_{v_0}$ determines the stopping distance similarly to $\mathcal{I}_{\hat{a}}$, as it stretches the possibly reachable positions farther from the start. This means the closest reachable position is defined by $v_{0,min}$ and $\hat{a}_{max}$, which stands for a very rough road-to-tire surface. In contrast, the

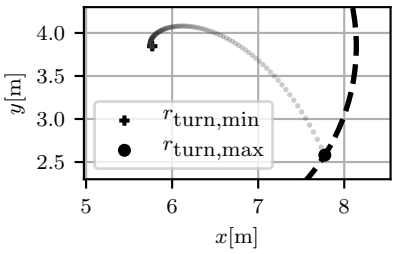

Figure 7. Effect of $\mathcal{I}_{r_{\text{turn}}}$ on X_{stop}. The figure shows how a circle can surround all stopping positions caused by different $r_{\text{turn}} \in \mathcal{I}_{r_{\text{turn}}} = [1\text{e}{-7}, 13]m$.

farthest reachable stopping position is defined by the highest velocity $v_{0,max}$ on the most slippery road $\hat{a}_{min}$ possible. An example of the resulting shape is shown in Figure 6b.

D. Initial position

The initial position of the vehicle will always be uncertain, as no perfect localization is possible. The effect of an uncertain starting position (x_0, y_0) is however not complex, as a different starting position of $\Delta x, \Delta y$ simply causes a translation of the complete reachable area of $\Delta x, \Delta y$.

E. Initial yaw angle

The initial yaw angle rotates the complete reachable area around the starting position of the vehicle. Figure 8a shows an example of this effect, where $\mathcal{I}_{\psi_0} = [-\pi/32, \pi/32]$.

F. Combination of all uncertainties

So far, we discussed the uncertainty of parameters separately. To describe and overestimate all system states that can potentially be reached under all uncertainties is not in the scope of this paper. In order to do so, a formal reachability analysis must be performed, compare for example [5][6][10][17].

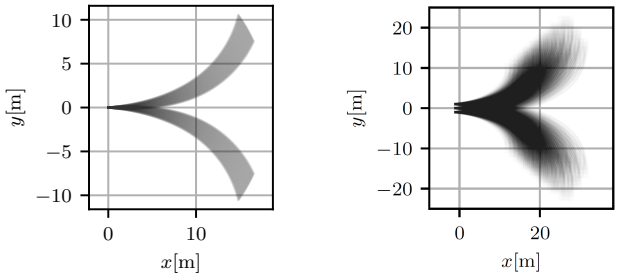

(a) Trajectories at interval $\mathcal{I}_{\psi_0} = [-\pi/32, \pi/32]$. Other parameters, $b = -0.6$, $\hat{a} = 4^m/_{s^2}$, $v_0 = 15.3^m/_s$, $r_{\text{turn}} = 12.5m$.

(b) Trajectories at interval $\mathcal{I}_{\hat{a}} = [7, 11]^m/_{s^2}$, $\mathcal{I}_{r_{\text{turn}}} = [7, 13]m$, $\mathcal{I}_{v_0} = [15.3, 18.1]^m/_s$, $\mathcal{I}_{\psi_0} = [-\pi/32, \pi/32]rad$, $\mathcal{I}_{x_0} = \mathcal{I}_{y_0} = [-1, 1]m$.

Figure 8. The effect of uncertain parameters. Left, only $\mathcal{I}_{\psi_0}$ is considered. Right, all parameters are assumed uncertain.

By sampling all parameters from $\mathcal{I}$ and calculating all combinations, we can estimate the reachable area non formally by the union of the resulting shapes. In Figure 8b we show such a result, where $\mathcal{I}_{\hat{a}} = [7, 11], \mathcal{I}_{r_{\text{turn}}} = [7, 13], \mathcal{I}_{v_0} = [15.3, 18.1], \mathcal{I}_{\psi_0} = [-\pi/32, \pi/32], \mathcal{I}_{x_0} = \mathcal{I}_{y_0} = [-1, 1]$. We sample 3 parameters of each interval.

 ISBN: 978-1-61208-720-7

IV. Conclusion

In this paper, we present a model for hard braking and collision avoiding vehicle trajectories. We take into account the maximally applicable acceleration/deceleration between tires and road surface, the minimal turning radius, the vehicle velocity, as well as starting position and heading. We explain our approach in detail and compare our model equations with an iterative CTRA-model simulation, which finds very similar solutions. However, in tests we could show that our solution computes stopping positions and trajectories up to 20 times faster than CTRA. By solving the compound differential equations for position in x, y-plane, we describe the complete vehicle motion till full stop, while also turning and still respecting the friction circle. With the derived equations, we can directly compute possible positions that a vehicle will reach in a braking and collision avoiding scenario. This might be used to generate braking and collision avoiding trajectories, by sampling our model for different feasible motion primitives, which can be computed in very short time.

We contribute a model that can aid in solving reachability problems for hard braking vehicles in an accurate and yet overapproximative way, considering all uncertainties in model parameters and start state of the vehicle.

As next steps, the proposed model for vehicle motion can be compared to the trajectories of real vehicles under the same assumptions given. Another next step might be the usage of our model for fast generation of braking trajectories by sampling motion primitives and compare the solution to other state of the art methods. As we can directly compute motion primitives for the highly non linear motions in braking and collision avoidance the proposed model can significantly reduce valuable trajectory generation time. Another aspect that can be tested is to apply our model in a formal reachability analysis for risk assessment in hard braking traffic scenarios and compare the solution to other contributions in the field of reachability analysis.

References

[1] M. Werling, J. Ziegler, S. Kammel, and S. Thrun, "Optimal trajectory generation for dynamic street scenarios in a frenet frame," in *Proceedings - IEEE International Conference on Robotics and Automation*, 06 2010, pp. 987 – 993.

[2] J. Ziegler, M. Werling, and J. Schröder, "Navigating car-like robots in unstructured environments using an obstacle sensitive cost function," in *IEEE Intelligent Vehicles Symposium, Proceedings*, 07 2008, pp. 787 – 791.

[3] C. Pek and M. Althoff, "Computationally efficient fail-safe trajectory planning for self-driving vehicles using convex optimization," in *Proc. of the IEEE Int. Conf. on Intelligent Transportation Systems*, 2018, pp. 1447–1454.

[4] S. Magdici and M. Althoff, "Fail-safe motion planning of autonomous vehicles," in *2016 IEEE 19th International Conference on Intelligent Transportation Systems (ITSC)*, Nov 2016, pp. 452–458.

[5] C. Pek, M. Koschi, and M. Althoff, "An online verification framework for motion planning of self-driving vehicles with safety guarantees," in *AAET - Automatisiertes und vernetztes Fahren*, 01 2019, pp. 260–274.

[6] I. M. Mitchell, "Comparing forward and backward reachability as tools for safety analysis," in *Hybrid Systems: Computation and Control*, A. Bemporad, A. Bicchi, and G. Buttazzo, Eds., 2007, pp. 428–443.

[7] E. Asarin, T. Dang, and A. Girard, "Reachability analysis of nonlinear systems using conservative approximation," in *Hybrid Systems: Computation and Control*, O. Maler and A. Pnueli, Eds., 2003, pp. 20–35.

[8] A. Girard, "Reachability of uncertain linear systems using zonotopes," in *Hybrid Systems: Computation and Control*, M. Morari and L. Thiele, Eds., 2005, pp. 291–305.

[9] M. Koschi and M. Althoff, "SPOT: A tool for set-based prediction of traffic participants," in *2017 IEEE Intelligent Vehicles Symposium (IV)*, June 2017, pp. 1686–1693.

[10] M. Althoff, "Reachability analysis and its application to the safety assessment of autonomous cars," Dissertation, Technische Universität München, München, 2010.

[11] B. Kim *et al.*, "Probabilistic vehicle trajectory prediction over occupancy grid map via recurrent neural network," *CoRR*, vol. abs/1704.07049, 2017.

[12] F. Giovannini, G. Savino, and M. Pierini, "Influence of the minimum swerving distance on the development of powered two wheeler active braking," in *22nd ESV Conference*, June 2011, paper 11-0258.

[13] C. Ackermann, J. Bechtloff, and R. Isermann, "Collision avoidance with combined braking and steering," in *6th International Munich Chassis Symposium 2015*, P. Pfeffer, Ed., 2015, pp. 199–213.

[14] C. Choi and Y. Kang, "Simultaneous braking and steering control method based on nonlinear model predictive control for emergency driving support," *International Journal of Control, Automation and Systems*, vol. 15, no. 1, pp. 345–353, Feb 2017.

[15] H. B. Pacejka, "Chapter 1 - Tire characteristics and vehicle handling and stability," in *Tire and Vehicle Dynamics (Third edition)*, H. B. Pacejka, Ed., 2012, p. 5.

[16] R. Schubert, E. Richter, and G. Wanielik, "Comparison and evaluation of advanced motion models for vehicle tracking," in *11th International Conference on Information Fusion*, June 2008, pp. 1–6.

[17] S. Söntges and M. Althoff, "Computing the drivable area of autonomous road vehicles in dynamic road scenes," *IEEE Transactions on Intelligent Transportation Systems*, vol. 19, no. 6, pp. 1855–1866, June 2018.

 ISBN: 978-1-61208-720-7